Journal of Civil Engineering and Urban Planning (2024)
Clausius Scientific Press, Canada

DOI: 10.23977/jceup.2024.060217
ISSN 2616-3969 Vol. 6 Num. 2

Vibration Response Analysis of Soil Mass in Shield Tunnel under Subway Load

Yi Ruyi[1], Ren Ruile[2]

[1]*Faculty of Architecture, Civil and Transportation Engineering, Beijing University of Technology, Beijing, 100142, China*
[2]*Key Laboratory of Urban Security and Disaster Engineering of the Ministry of Education, Beijing, 100142, China*

Keywords: Shield tunnels; train loads; Infinite Element; numerical simulation; Power response

Abstract: As the medium of train vibration propagation, it is an important basis to study the vibration of the surrounding environment to clarify the propagation attenuation law of train-induced vibration in the formation.In this paper, a refined three-dimensional finite element numerical model of the overall track bed-lining structure-stratum is established, the train load is simplified into a series of moving excitations, and the train moving load is linked with the ABAQUS program through the Dload subprogram to realize the application of the train load, which reveals the vertical and horizontal vibration response laws of the soil and lining structure around the tunnel caused by the train vibration load, and analyzes the influence of different train running speeds on the vibration propagation law.The results show that in the lining structure between the central axes of the two rails, the vibration acceleration reaches the maximum, and the horizontal vibration caused by the vertical vibration load cannot be ignored; for the vertical vibration, the attenuation rate is 65%-70% from the tunnel wall R along the soil layer above the tunnel vault and below the tunnel bottom; for the horizontal vibration, the attenuation rate of the soil layer along the tunnel waist is about 35% in the range of R from the tunnel wall; and the vibration acceleration decreases significantly with the increase of train speed.

1. Introduction

With the continuous improvement of social and economic level, China's rail transit construction has developed rapidly, among which, the mileage of urban rail transit has reached 10 165.7 kilometers, and will reach 13,000 kilometers by the end of the 14th, 000 kilometers. The resulting environmental vibration, operation safety and other problems are increasingly prominent.

At present, many scholars have carried out a lot of research on the vibration load of subway train and its impact on environmental vibration. In terms of vehicle vibration load research, Wang Xiangqiu et al. [1] used advanced test instruments to conduct field tests on the dynamic response of Zhuting tunnel structure of Beijing-Guangzhou Line, and gave the numerical definite expression of train dynamic load. Gao Feng et al. [2] obtained the numerical expression of train vibration load based on the acceleration data of train vibration field test in Zhalanyingzi Tunnel of Beijing-Tongliao Line and

the analysis of train vehicle system vibration. Liu Weining[3]. The vibration load of the train was determined by establishing the vibration response analysis model of the vehicle-track foundation-lining structure-formation system. Du Lin Lin[4]. According to the curve section of the subway line, the vibration response model of the curve track section is established in the frequency domain, and the vibration source of the subway train in different states of the curve track is obtained. Some scholars gave the test vibration load, based on the field test data, such as Pan Changji[5]. We first proposed the numerical expression of train dynamic load, which is composed of a single static load and three sine functions, beam wave[6]. On this basis, the mutual superposition of the adjacent wheels, the dispersion and the rotation excitation and other elements, and the existing train load expressions are corrected and perfected.

To sum up, most of the existing vehicle-induced vibration related studies focus on the impact of high-speed railway subgrade vibration on the surrounding structure, and the research of underground rail transit operation on the surrounding environment is not perfect. In particular, the analysis of the vibration response in the vehicle-track-lining-formation integral system is rarely reported. As the medium of vibration propagation, it is an important basis to study the vibration of the surrounding environment.

This paper established the whole channel bed-lining structure-formation fine three-dimensional finite element numerical model, analyzes the train vibration load around the tunnel soil and lining structure of vertical and horizontal vibration response rule, studied the influence of different train speed on vibration propagation law, the design of subway and operation maintenance has great significance.

2. Construction of the numerical model

2.1 Finite element model

In this paper, a 3 D numerical analysis model of integral channel bed-lining structure-formation refinement is established based on the ABAQUS finite element platform. The site length is 90 m, the width is 30 m, the depth is 60 m, the tunnel diameter is 8.8 m, the length is 90 m, the buried depth of the tunnel center is 30 m, so as to observe the complete attenuation law of vehicle vibration in all directions. The details of the 3 D finite element model and the integral channel bed-lining-soil system are shown in Figure 1 and Figure 2.

It has been shown that[7]. Subway vibration load attenuation is fast, and the load is relatively small. Since the tunnel lining structure and the surrounding soil are basically within their elastic range, a 3D finite element model of the bed-lining structure-formation is established. In this model, all materials are assumed to be linearly elastic. The soil units and rail structure units are simulated using solid units. The lining's outer surface is in contact with the soil body surface, forming a binding relationship. A total of 90,160 grid units are included in the model. The basic material parameters of the soil and structure are shown in Table 1 and Table 2.

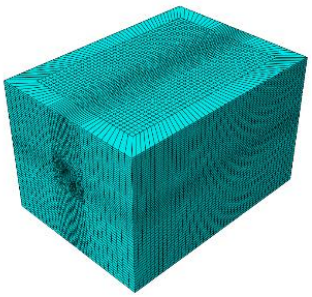

Figure 1: Track-tunnel-soil finite element model

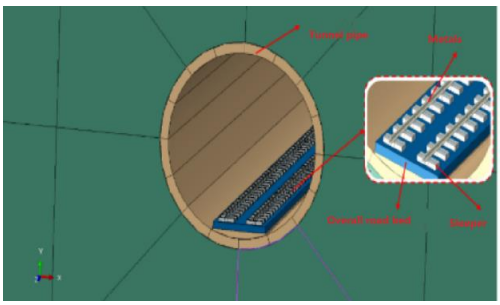

Figure 2: Detail of the track bed-tunnel-soil

Table 1: Basic parameters of soil

soil body	Elastic modulus / MPa	Poisson ratio	density kg/m^3
sandy soil	300	0.49	1749

Table 2: Basic parameters of structure

Tunnel structure	material	density g/cm^3	Elastic modulus / MPa	Poisson ratio
ballast bed	C 35 for concrete	2500	$.63\times10^4$	0.2
rail	T 60 steel	7850	$.062\times10^5$	0.3
lining	C50 concrete	2700	3×10^4	0.3

2.2 Infinite-element boundary conditions and other settings

During dynamic loading, considering the problem of fluctuation propagation, the truncation boundary does not conform to the reflection of actual fluctuations, and the analysis results will be disturbed, so this model uses infinite element boundary simulation to eliminate the influence of fluctuation reflection.

The model is a 3 D model, so the unit is mainly hexahedral units, forming the model on the basis of hexahedral units. The inp file, the model left and bottom areas by modification. The keyword in the inp file changes the hexahedral unit to an infinite metaelement that extends away. The left and right sides of the infinite element boundary and the lower width are taken as 10 m each.

2.3 Train load

According to domestic scholar Pan Changji[5] and the research of domestic scholar Pan Changji et al. [5], the artificial excitation force function of the vertical load of the train is composed of the static load of the train wheel and a series of sinusoidal functions. The expression is as follows:

$$F(t) = P_0 + P_1 \sin(\omega_1 t) + P_2 \sin(\omega_2 t) + P_3 \sin(\omega_3 t) \tag{1}$$

among,

$$P_i = M_0 \alpha_i \omega_i^2 \quad (i = 1,2,3) \tag{2}$$

$$\omega_i = 2\pi v / L_i \quad (i = 1,2,3) \tag{3}$$

In formula: P_0For a single wheel static load; P_1,P_2,P_3. The typical vibration load values of three control conditions according to ride comfort, power additional load on the line and rail surface wear; ω_iIs the circular frequency of the uneven vibration wavelength corresponding to the train speed v; M_0The unsprung mass of the train; Table 3 shows the calculated parameters under the three control conditions when the running speed is 72 km/h$_i$For a typical vector height, L, under the 3 control conditions in Table 3$_1$Is a typical wavelength corresponding to the 3 control conditions in Table 3, and t is the time.

This paper uses the type B EMU. Bring the parameters into formula (1) (2) (3) to calculate the corresponding speed load expression of subway train as formula (4), and its load time curve is shown in Figure 3.

Table 3: The value of the excitation force function is calculated

controlling condition	unsprung weight M_0/kg	speed of a motor vehicle v /(km/h)	wavelength L /m	rise a /mm	circular frequency w /s^{-1}
1	1350	72	10	3.5	12.56
2	1350	72	2	0.4	62.8
3	1350	72	0.5	0.08	251.2

$$F(t) = 73867 + 745.39\sin(12.56t) + 2129.67\sin(62.8t) + 6814.96\sin(251.2t) \quad (4)$$

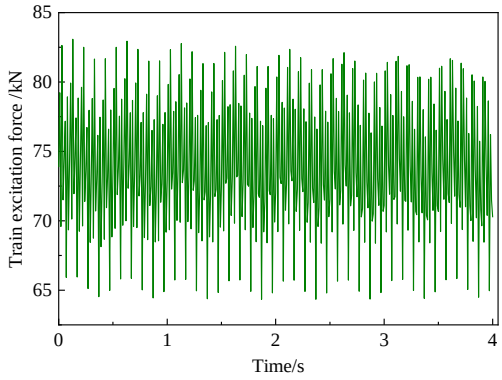

Figure 3: Loading time-history curve of subway trains

2.4 Application of train vibration load

To simulate the movement of the above vehicle load on the track, the Dload subroutine is secondary developed in the ABAQUS software. In this paper, the train load is directly applied to the train rail, and the train load only considers a single carriage.

With the help of the dynamic model established above, the law of soil vibration around the tunnel caused by subway operation is studied. In this paper, the train running speed is 72 km/h, mainly studying the following contents: (1) the dynamic response law of the tunnel lining structure; (2) the vertical propagation law of vibration in the surrounding soil; and (3) the horizontal propagation law of vibration in the surrounding soil. The tunnel radius is R, and the observation points selected in the study are shown in Figures 4 and 5. Where Figure 4 shows the observation sites in the surrounding soil, and Figure 5 shows the observation sites in the lining.

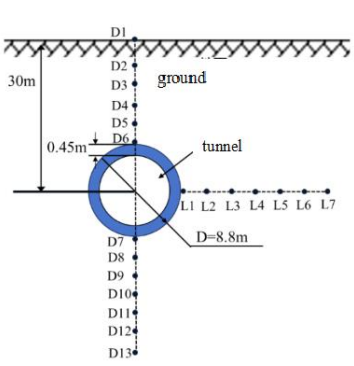

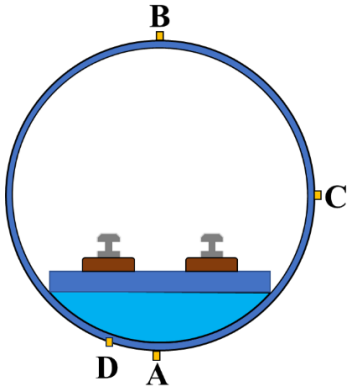

Figure 4: Schematic diagram of the location of model observations (Left)

Figure 5: Schematic diagram of Lining observation point arrangement (Right)

3. The propagation law of vehicle vibration in the lining structure

Figure 6 shows the vibration acceleration vector diagram of the lining caused by vehicle vibration position, including figure 6 (a) shows the vertical vibration acceleration vector diagram, from figure 6 (a), the rail axis D point, lining vertical vibration acceleration, and overall in the two vertical acceleration in the lining between the rail axis, the top, the waist vertical acceleration is the smallest. Figure 6 (b) shows the horizontal vibration acceleration vector diagram. From Figure 6 (b), the vertical vibration load produces the horizontal vibration in the lining structure, and the horizontal vibration acceleration at the lining waist position reaches 0.130 m / s^2, About 1.9 times the maximum value of the vertical vibration acceleration here, and the horizontal vibration acceleration near the central axis (point D) of the rail is also 0.214 m / s^2It is seen that the horizontal vibration acceleration caused by vertical excitation still cannot be ignored. Figure 6 (c) shows the vector diagram of the vibration total acceleration. As can be seen from Figure 6 (c), the vibration acceleration of the lining structure is concentrated at the intersection of the central axis of the two rails, and the acceleration distribution of the other positions is relatively uniform.

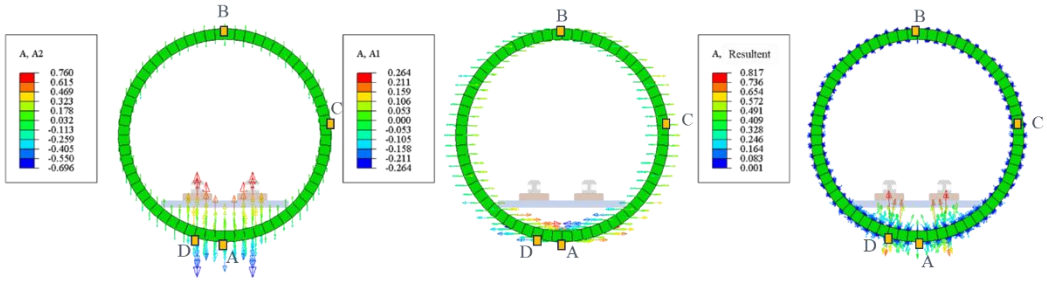

(A) Vertical acceleration vector diagram (B) Horizontal acceleration vector plot (C) Diagram of the total acceleration vector

Figure 6: Lining acceleration vector diagram

Fig. 7 specifically presents the vertical vibration acceleration time course curve at different positions A, B, C, D of the lining. It can be observed that, due to the impact of the train load, the bottom lining is the most directly affected area, with the vertical acceleration value at monitoring point D being the highest, reaching 0.552 m/s². The peak vertical acceleration at point A, located at the bottom of the lining, is 0.472 m/s². However, at the top of the lining, the vertical acceleration value at point B decreases significantly to 0.108 m/s², and it reaches a minimum at point C, measuring 0.067 m/s². When compared to point D, the decay rate is 87.8%. Figure 8 shows the vertical acceleration frequency curve at different positions of the lining. As can be seen from the figure, the main frequency of each position of the lining structure is concentrated in two sections, the first section is mainly concentrated in 1 Hz ~10 Hz, and the second section is concentrated in 25 Hz ~40 Hz. The energy of both frequency bands needs to be focused on.

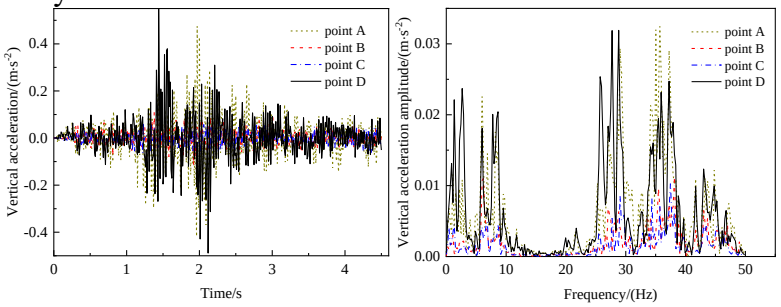

Figure 7: Time history curves of ground acceleration at different velocities (Left)

Figure 8: Ground acceleration range curves at different velocities (Right)

4. Analysis of the propagation law of vehicle-induced vibration in the surrounding soil

4.1 Analysis of the vertical vibration propagation law in the strata above the tunnel vault

Figure 9 illustrates the vibration propagation law of the vehicle's vibration as it traverses the soil roof above the vault. Specifically, it demonstrates that at the monitoring point, the vibration decays most rapidly from D6 to D5. In numerical terms, the acceleration decreases from 0.05 m/s² at a distance of twice the tunnel vault's radius, R, to 0.015 m/s², resulting in a decay rate of 70%.

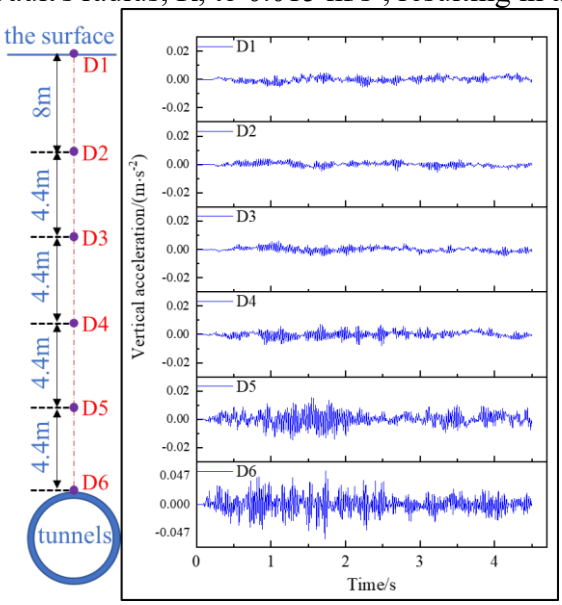

Figure 9: Characteristics of vibration distribution in the strata above the tunnel vault

Figure 10 shows the vibration acceleration spectrum of soil at each position of the monitoring point D 1-D 5. As can be seen from the figure, the range of the main vibration frequency band at each position is roughly the same, and there is only one obvious peak, and the main vibration frequency of the acceleration is concentrated at about 35 Hz.

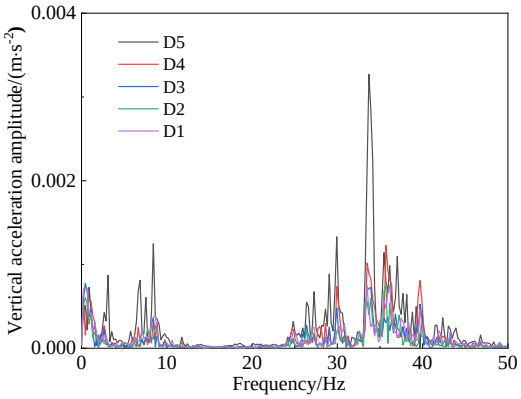

Figure 10: Frequency range curves of each position of the soil layer above the tunnel vault

4.2 Analysis of the propagation law of vertical and horizontal vibration in the waist soil of the tunnel

Figure 11 shows the vibration vertical and horizontal acceleration distribution diagram at each position of the tunnel waist soil layer. As can be seen from Figure 11 (a), the maximum vertical

acceleration at L1 is 0.026 m/s2, while the maximum vertical acceleration at L2 is 0.0178 m/s2. The decay rate reaches 34% within twice the tunnel radius, and the vertical acceleration at point L7, located 6R away from the tunnel waist, decreases to 0.0036 m/s2. Similarly, Figure 11 (b) reveals that the maximum horizontal acceleration at L1 is 0.030 m/s2, while the maximum horizontal acceleration at L2 is 0.020 m/s2. The horizontal vibration decay rate within the radius of the tunnel reaches 33%, and the horizontal acceleration at point L7, located at the waist 60R away, decreases to 0.002 m/s2.

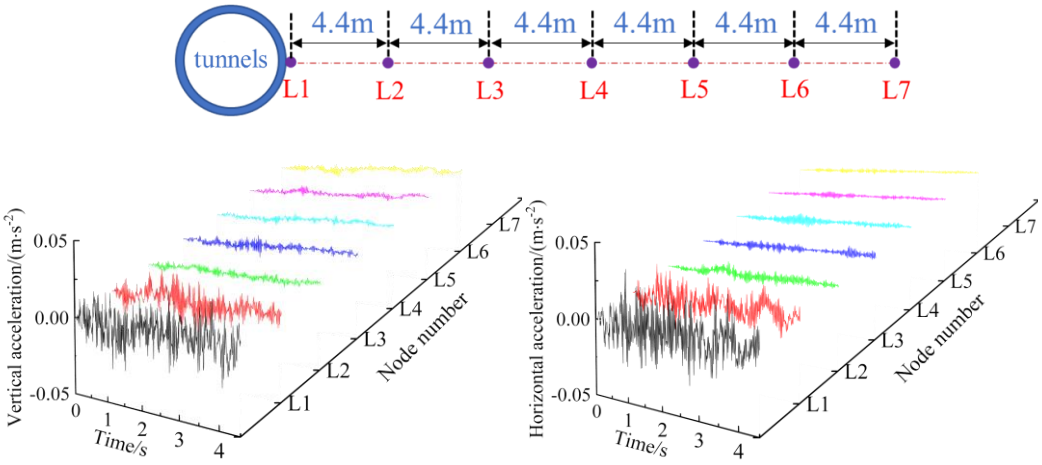

(A) Time-course curve of the vertical acceleration distribution (B) Time-course curve of the horizontal acceleration distribution

Figure 11: Distribution of vibration acceleration at each position of the soil layer at the waist of the tunnel

Figure 12 and Figure 13 respectively show the vertical and horizontal vibration acceleration frequency spectra of the soil at each position of the L2-L7 monitoring point. It can be seen from the figure that the vibration energy at each position is mainly concentrated at 35Hz.

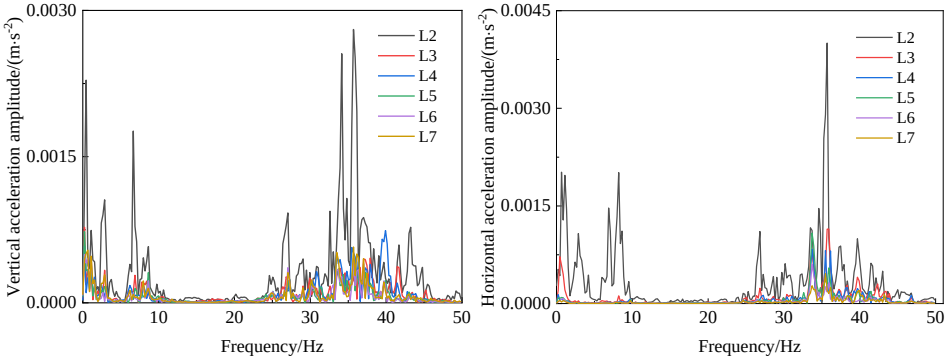

Figure 12: Vertical acceleration frequency range curves of each position of the soil layer at the waist of the tunnel (Left)

Figure 13: Horizontal acceleration frequency range curves of each position of the soil layer at the waist of the tunnel (Right)

4.3 Analysis of the vertical vibration propagation law in the strata below the bottom of the tunnel

Figure 14 shows the distribution characteristics of the vibration of the soil below the bottom of the tunnel when the train passes. It can be seen from the figure that the fastest decay within R from the bottom of the tunnel occurs from 0.29 m/s at D72 to 0.098 m/s2, which represents a decrease of 66%.

When the vibration propagated to 5R from the base, the peak acceleration value decayed to 0.024 m/s2, resulting in a decay rate of 91%. Comparing figures 14 and 9, the vibration acceleration is obviously different between the upward propagation and the downward propagation in the soil layer, and the vibration acceleration amplitude of the downward propagation is about 5~6 times of the vibration acceleration amplitude of the upward propagation.

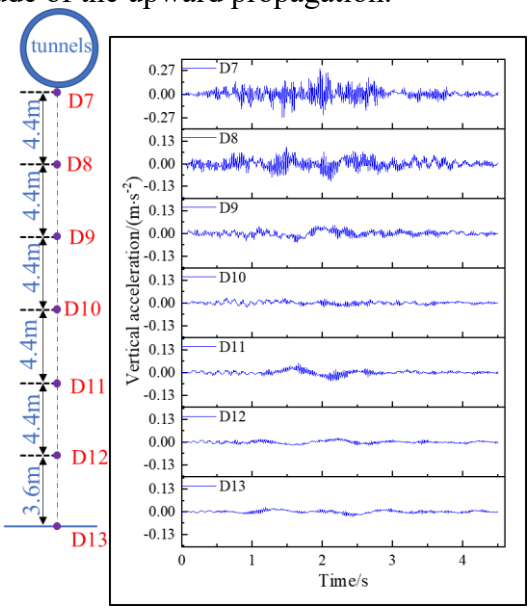

Figure 14: Characteristics of the vibration distribution of the strata below the tunnel

FIG. 15 shows the frequency spectrum obtained by Fourier transform of the vibration acceleration of the soil below the bottom of the tunnel. As can be seen from the figure, the main vibration frequency band at each position is roughly the same range, mainly between 32 Hz and 37 Hz.

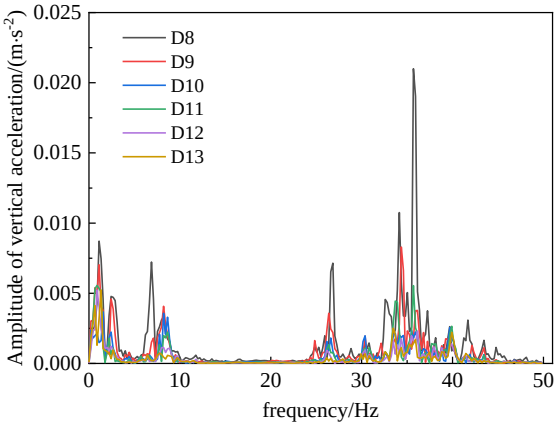

Figure 15: Frequency range curves of each position of the soil layer below the tunnel

5. Influence of train running speed on vibration response

Figures 16 and 17 show the decay law of the vertical acceleration maximum along the vertical propagation at three train speeds. As can be seen from the figure, with the increase of the train speed, the maximum vertical acceleration in the soil layer gradually decreases, and both are at the tunnel radius position, the vertical acceleration decay rate reaches 65%~75%, and the attenuation rate basically reaches 82%~87%.

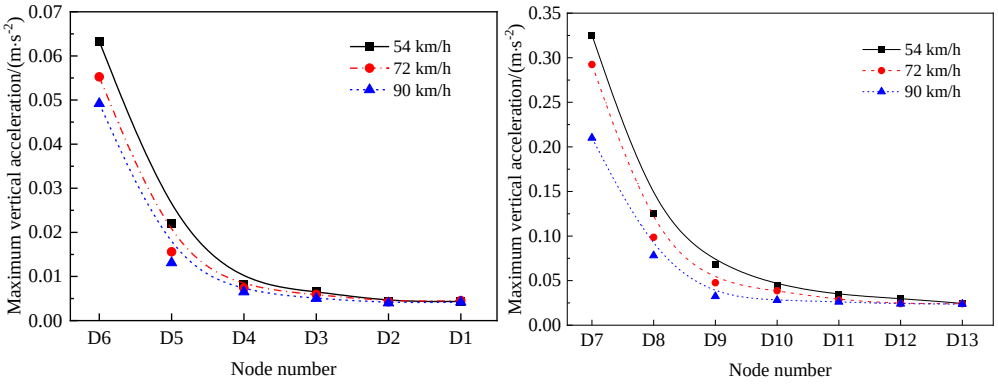

Figure 16: Attenuation law of peak vertical acceleration of soil above tunnel vault (Left)

Figure 17: Attenuation law of vertical acceleration peak of soil mass below tunnel bottom (Right)

Figures 18 and 19 show the attenuation rules of vertical and horizontal acceleration in the waist soil in the tunnel at different train speeds. Similarly, it can be seen from the figure that with the increase of the train running speed, the vibration acceleration in the soil around the tunnel is significantly reduced and the waist acceleration of the tunnel from the monitoring point L1 to L2, that is, the radius of a tunnel can reach 25%~40% (the decay rate is about 75%~85% ~ 85% within 2R. Under the three types of trains, the vibration acceleration in the formation basically decreases to 0 at 6R from the tunnel wall.

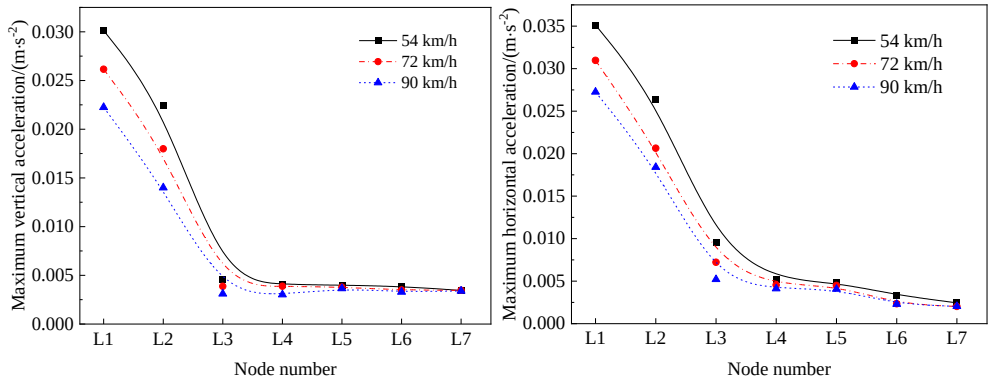

Figure 18: Attenuation law of vertical acceleration peak of soil in tunnel waist (Left)

Figure 19: Attenuation law of peak horizontal acceleration of soil in tunnel waist (Right)

6. Conclusion

In this paper, the finite element software Abaqus establishes the integral channel bed-lining-soil system, develops the train load with Dload subprogram to the rail, studies the propagation law of vehicle-induced vibration in the tunnel lining and the surrounding soil, and obtains the following understanding:

(1) The vibration of the lining in the lining structure between the central axis of the maximum, the top, the smallest tunnel waist, the lining waist dynamic response decreased 87.8% compared to the bottom of the tunnel, the lining in the main frequency band concentrated around 1 Hz ~10 Hz and 25 Hz~40 Hz.

(2) For vertical vibration, the decay rate along the soil layer above the tunnel vault and the soil layer below the bottom of the tunnel is 65%~70%; for horizontal vibration, the decay rate along the waist of the tunnel is about 35%; the acceleration frequency at each position of the soil body is mainly about 35Hz.

(3) At the same position of the soil layer, the vertical acceleration shows a decreasing trend with the increase of the velocity. Moreover, this change is significant in the distance from the tunnel wall R. With the increase of the distance, the vibration acceleration corresponding to different velocities is basically not different.

References

[1] Wang Xiangqiu, Yang Linde, Gao Wenhua. Railway tunnel acceleration train vibration test and load simulation [J]. Vibration and Impact, 2005, (03): 99-102 + 107-138.

[2] Gao Feng. Analysis of train vibration response in railway tunnel [J]. Journal of Lanzhou Railway College, 1998, (02): 7-13.

[3] Liu Weining, Xia He, Guo Wenjun. Environmental response of subway train vibration [J]. Journal of Rock mechanics and Engineering, 1996, (S1): 586-593.

[4] Linlin Du. Analytical model of rail coupling and vibration source characteristic of subway train curve operation [D]. Beijing: Beijing Jiaotong University, 2018

[5] Pan Changji, Li Dewu, Xie Zhengguang. Discussion on the environmental impact of subway train vibration in Beijing [J]. Vibration and shock, 1995, (04): 29-34 + 78.

[6] Liang Bo, Luo Hong, Sun Changxin. Simulation of vibrational loads in high-speed railways [J]. Railway Journal, 2006, (04): 89-94.

[7] Yan Weiming, Nie Han, Ren Min, et al. Measurement and analysis of ground vibration caused by subway traffic [J]. Journal of Railway Science and Engineering, 2006, (02): 1-5